

NeuralLift-360: Lifting An In-the-wild 2D Photo to A 3D Object with 360° Views

Dejia Xu, Yifan Jiang, Peihao Wang, Zhiwen Fan, Yi Wang, Zhangyang Wang
 University of Texas at Austin
 {dejia,atlaswang}@utexas.edu

Abstract

*Virtual reality and augmented reality (XR) bring increasing demand for 3D content. However, creating high-quality 3D content requires tedious work that a human expert must do. In this work, we study the challenging task of lifting a single image to a 3D object and, for the first time, demonstrate the ability to generate a plausible 3D object with 360° views that corresponds well with the given reference image. By conditioning on the reference image, our model can fulfill the everlasting curiosity for synthesizing novel views of objects from images. Our technique sheds light on a promising direction of easing the workflows for 3D artists and XR designers. We propose a novel framework, dubbed **NeuralLift-360**, that utilizes a depth-aware neural radiance representation (NeRF) and learns to craft the scene guided by denoising diffusion models. By introducing a ranking loss, our NeuralLift-360 can be guided with rough depth estimation in the wild. We also adopt a CLIP-guided sampling strategy for the diffusion prior to provide coherent guidance. Extensive experiments demonstrate that our NeuralLift-360 significantly outperforms existing state-of-the-art baselines. Project page: <https://vita-group.github.io/NeuralLift-360/>*

1. Introduction

Creating 3D content has been a long-standing problem in computer vision. This problem enables various applications in game studios, home decoration, virtual reality, and augmented reality. Over the past few decades, the manual task has dominated real scenarios, which requires tedious professional expert modeling. Modern artists rely on special software tools (e.g., Blender, Maya3D, 3DS Max, etc.) and time-demanding manual adjustments to realize imaginations and transform them into virtual objects. Meanwhile, automatic 3D content creation pipelines serve as effective tools to facilitate human efforts. These pipelines typically capture hundreds of images and leverage multi-view stereo [71] to quickly model fine-grained virtual landscapes.

More recently, researchers have started aiming at a more

ambitious goal, to create a 3D object from a single image [9, 10, 12, 21, 27, 51, 66, 68]. This enables broad applications since it greatly reduces the prerequisite to a minimal request. Existing approaches can be mainly categorized into two major directions. One line of work utilizes learning priors from large-scale datasets with multi-view images [10, 21, 51, 66, 68]. These approaches usually learn a conditional neural network to predict 3D information based on input images. However, due to their poor generalization ability, drastic performance degradation is observed when the testing image is out-of-distribution.

Another direction constructs the pipeline on top of the depth estimation techniques [65]. Under the guidance of monocular depth estimation networks [43, 44], the 2D image is firstly back-projected to a 3D data format (e.g., point cloud or multi-plane image) and then re-projected into novel views. After that, advanced image inpainting techniques are then adopted to fill missing holes [52] produced during the projection. However, most of them can be highly affected by the quality of the estimated depth maps. Though LeRes [73] attempted to rectify the predicted depth by refining the projected 3D point cloud, their results do not generalize well to an arbitrary image in the wild. Overall, the aforementioned approaches are either adopted in limited scenarios (e.g. face or toy examples [4, 75]), or only produce limited viewing directions [8, 70] when being applied to scenes in the wild. Different from all these approaches, we focus on a more challenging task and for the first time, show promising results by **lifting a single in-the-wild image into a 3D object with 360° novel views**.

Attracted by the dramatic progress of neural volumetric rendering on 3D reconstruction tasks, we consider building our framework based on Neural Radiance Fields (NeRFs) [35]. The original NeRF takes hundreds of training views and their camera poses as inputs to learn an implicit representation. Subsequent models dedicate tremendous efforts [8, 19, 70, 75] to apply NeRF to sparse training views. The most similar work [70] to our method proposes to optimize a NeRF using only a single image and its corresponding depth map. However, it renders limited views from a small range of angles, and the prerequisite of a high-quality

depth map largely constrains its practical usage.

To address the above issues, we propose a novel framework, coined as **NeuralLift-360**, which aims to ease the creation of 3D assets by building a bridge to convert diverse in-the-wild 2D photos to sophisticated 3D contents in 360° views and enable its automation. The major challenge in our work is that the content on the back side is hidden and hard to hallucinate. To tackle these hurdles, we consider the diffusion priors together with the monocular depth estimator as the cues for hallucination. Modern diffusion models [41, 48, 50] are trained on a massive dataset (e.g., 5B text-to-image pairs [24]). During inference time, they can generate impressive photorealistic photos based on simple text inputs. By adopting these learning priors with CLIP [40] guidance, NeuralLift-360 can generate plausible 3D consistent instances that correspond well to the given reference image while only requiring minimal additional input, the correct user prompts. Moreover, rather than simply taking the depth map from the pre-trained depth estimator as geometry supervision, we propose to use the relative ranking information from the rough depth during the training process. This simple strategy is observed to robustly mitigate geometry errors for depth estimations in the wild.

Our contributions can be summarized as follows,

- Given a single image in the wild, we demonstrate promising results of them being lifted to 3D. We use NeRF as an effective scene representation and integrate prior knowledge from the diffusion model.
- We propose a CLIP-guided sampling strategy that effectively marries the prior knowledge from the diffusion model with the reference image.
- When the reference image is hard to describe exactly, we finetune the diffusion model on the single image while maintaining its ability to generate diverse contents to guide the NeRF training.
- We introduce scale-invariant depth supervision that uses the ranking information. This design alleviates the need for accurate multi-view consistent depth estimation and broadens the application of our algorithms.

2. Related Works

2.1. 3D from Single Image

Inferring 3D worlds from a single image has been a popular direction over the past years. Previous works try to solve this problem by firstly adopting a monocular depth estimator (e.g., MiDaS [44]) to predict the 3D geometry and then using multi-plane images (MPI) [20, 52] or point cloud [36] to render artistic effects. Meanwhile, the missing

holes from novel views are inpainted by a pre-trained modern deep network [76]. While these approaches are powerful and efficient, the depth estimator could be unstable, and the inpainting techniques may produce artifacts that make the rendered images look fake. While our method also applies a monocular depth estimator as the geometry cues, we propose a depth ranking loss that can mitigate the instability of depth estimation in the wild. Later approaches [28, 75] train their model on a large-scale 3D assets dataset. During inference time, they directly predict a 3D object using a single image. However, their performance faces drastic degradation when being applied to an in-the-wild image, due to the domain gap. The most similar work to ours is SinNeRF [70], which trains a neural radiance field only on a single RGB image and its corresponding depth map. However, their approach requires a high-quality depth map for geometry guidance, and it can only render views from a small range of angles. Thanks to the proposed depth ranking loss, our method can reconstruct impressive geometry information only using guidance from a pre-trained monocular depth estimator.

2.2. Neural Radiance Fields

Neural Radiance Fields (NeRFs) [34] have shown encouraging performance for view synthesis. After its origin, tremendous efforts have been devoted to improving it [2, 3, 5, 6, 11, 14, 16, 18, 31, 37, 45, 57, 59, 61, 63, 67, 75]. Unlike most NeRF-like models, which at least require several different views to reconstruct scenes, we focus on reconstructing 3D content with single views. Analogously, recent works [18, 39] try to generate 3D content from text inputs directly. Although they also rely on the text prompt as guidance, their rendered objects are only conditioned on text sentences without image constraints, which can not reach our goal. Different from them, we aim at lifting a single image (either real or synthetic) to photorealistic 3D objects.

3. Preliminaries

Neural Radiance Field Neural Radiance Fields (NeRFs) [34] render images by sampling 5D coordinates (location (x, y, z) and viewing direction (θ, ϕ)) along camera rays. After mapping them to color (r, g, b) and volume density σ , additional volumetric rendering techniques are adopted to fuse the information along the ray. Given \mathbf{o} as the camera origin and \mathbf{d} as the ray direction, 3D point locations along the ray can be expressed as $\mathbf{r}(t) = \mathbf{o} + t\mathbf{d}$. The predicted color accumulated is defined as follows:

$$\mathbf{C}(\mathbf{r}) = \int_{t_n}^{t_f} T(t)\sigma(\mathbf{r}(t))\mathbf{c}(\mathbf{r}(t), \mathbf{d})dt, \quad (1)$$

where $T(t) = \exp\left(-\int_{t_n}^t \sigma(\mathbf{r}(s))ds\right)$, $\sigma(\cdot)$ and $\mathbf{c}(\cdot, \cdot)$ are densities and color predictions. To numerically evaluate

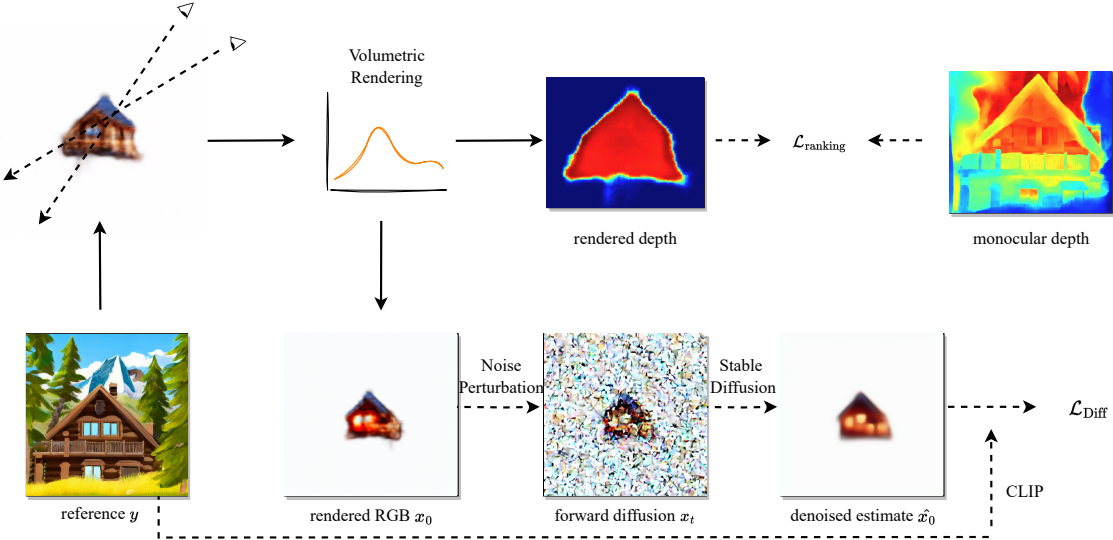


Figure 1. Overview of our pipeline. Our NeuralLift-360 learns to recover a 3D object from a single reference image y . We derive a prior distillation loss $\mathcal{L}_{\text{diff}}$ for CLIP-guided diffusion prior and utilize rough depth estimation in the wild with the help of a ranking loss $\mathcal{L}_{\text{ranking}}$.

Eq. 1, the continuous integral is estimated using quadrature [34]. When rendering a view, NeRF enumerates all the rays cast from pixels on the image plane, and pixel-wisely renders each ray using Eq. 1. Our model is built upon Instant-NGP [37], which reduces computation cost by inferring color and density from a multiresolution hash table implemented by CUDA.

Denoising Diffusion Model Denoising diffusion models generate images by gradually denoising from a gaussian noise $p(\mathbf{x}_T) = \mathcal{N}(\mathbf{0}, \mathbf{I})$ and transforming into a certain data distribution. The forward diffusion process $q(\mathbf{x}_t | \mathbf{x}_{t-1})$ adds Gaussian noise to the image \mathbf{x}_t . The marginal distribution can be written as: $q(\mathbf{x}_t | \mathbf{x}_0) = \mathcal{N}(\alpha_t \mathbf{x}_0, \sigma_t^2 \mathbf{I})$, where α_t and σ_t are designed to converge to $\mathcal{N}(\mathbf{0}, \mathbf{I})$ when t is at the end of the forward process [23, 56]. The reverse diffusion process $p(\mathbf{x}_{t-1} | \mathbf{x}_t)$ learns to denoise. Given infinitesimal timesteps, the reverse diffusion process can be approximated with Gaussian [56] related with an optimal MSE denoiser [53].

The diffusion models are designed as noise estimators $\epsilon_\theta(\mathbf{x}_t, t)$ taking noisy images as input and estimating the noise. They are trained via optimizing the weighted evidence lower bound (ELBO) [17, 23]:

$$\mathcal{L}_{\text{ELBO}}(\theta) = \mathbb{E} \left[w(t) \|\epsilon_\theta(\alpha_t \mathbf{x}_0 + \sigma_t \epsilon; t) - \epsilon\|_2^2 \right], \quad (2)$$

where $\epsilon \sim \mathcal{N}(\mathbf{0}, \mathbf{I})$, $w(t)$ is a weighting function. In practice, setting $w(t) = 1$ delivers good performance [17]. Sampling from a diffusion model can be either stochastic [17] or deterministic [54]. After sampling $\mathbf{x}_T \sim \mathcal{N}(\mathbf{0}, \mathbf{I})$, we can gradually reduce the noise level and reach a clean image with high quality at the end of the iterative process.

4. Method

Overview. In this section, we propose our method, dubbed NeuralLift-360, which reconstructs a 3D object from a single image. An overview of NeuralLift-360 is illustrated in Fig. 1. NeuralLift-360 combines the best of the two worlds: NeRF and diffusion model, where the former is leveraged to universally model a 3D scene, while the latter is utilized to hallucinate the unseen views. To inject knowledge of a diffusion model into a radiance field, we derive a training framework in Sec. 4.1, whose supervision consists of two parts: (1) a prior distillation loss from a generative model (Sec. 4.2), (2) a straight loss on the given image (Sec. 4.4). Moreover, we introduce a domain adaption technique to adapt the diffusion prior to in-the-wild images (Sec. 4.3).

4.1. Probabilistic-Driven 3D Lifting

We begin by formulating our setting along the way, introducing our notations. Given an image $\mathbf{y} \in \mathbb{R}^N$ and its text description $\mathbf{z} \in \mathbb{R}^D$, NeuralLift-360 intends to reconstruct a 3D scene $\mathbf{V} \in \mathbb{R}^M$, where \mathbf{V} can be either a radiance volume or the network parameters of a NeRF. We regard \mathbf{y} , \mathbf{z} and \mathbf{V} as random variables. To reconstruct \mathbf{V} from \mathbf{y} and \mathbf{z} , we maximize a log-posterior and apply Bayesian rule:

$$\log p(\mathbf{V} | \mathbf{y}, \mathbf{z}) = \log p(\mathbf{y} | \mathbf{V}, \mathbf{z}) + \log p(\mathbf{V} | \mathbf{z}) + C, \quad (3)$$

where C is the evidence term, a constant. One can see the prior term $p(\mathbf{V} | \mathbf{z})$ provides complementary information to lift an image into 3D space. However, specifying this prior can be intractable, and directly optimizing objective Eq. 3 is also sampling inefficient. Instead, we introduce camera pose $\Phi \in \mathbb{SO}(3) \times \mathbb{R}^3$ as a latent variable, then the likeli-

hood term can be rewritten as:

$$p(\mathbf{y}|\mathbf{V}, \mathbf{z}) = \int p(\mathbf{y}|\mathbf{V}, \Phi, \mathbf{z})p(\Phi|\mathbf{V}, \mathbf{z})d\Phi \quad (4)$$

$$= \int p(\mathbf{y}|\mathbf{V}, \Phi, \mathbf{z}) \frac{p(\mathbf{V}|\Phi, \mathbf{z})p(\Phi)}{p(\mathbf{V}|\mathbf{z})} d\Phi. \quad (5)$$

Merging Eq. 3 and Eq. 5, we can get rid of the implicit prior term and obtain a sampling efficient ELBO of the original objective as below:

$$\log \mathbb{E}_{\Phi \sim p(\Phi)} p(\mathbf{y}|\mathbf{V}, \Phi, \mathbf{z})p(\mathbf{V}|\Phi, \mathbf{z}) \quad (6)$$

$$\geq \mathbb{E}_{\Phi \sim p(\Phi)} [\log p(\mathbf{y}|\mathbf{V}, \Phi, \mathbf{z}) + \log p(\mathbf{V}|\Phi, \mathbf{z})]. \quad (7)$$

Furthermore, we define $p(\mathbf{y}|\mathbf{V}, \Phi, \mathbf{z}) = p(\mathbf{y}|h(\mathbf{V}, \Phi), \mathbf{z})$ and $p(\mathbf{V}|\Phi, \mathbf{z}) = p(h(\mathbf{V}, \Phi)|\mathbf{z})$, where $h(\mathbf{V}, \Phi)$ renders the 3D scene with respect to the camera pose Φ . Then we derive our final training objective for NeuralLift-360:

$$\mathcal{L} = -\mathbb{E}_{\Phi} \left[\underbrace{\log p(\mathbf{y}|h(\mathbf{V}, \Phi), \mathbf{z})}_{\text{referenced loss}} + \underbrace{\log p(h(\mathbf{V}, \Phi)|\mathbf{z})}_{\text{non-referenced loss}} \right]. \quad (8)$$

At each training step, we sample a camera pose with respect to a distribution (more on Sec. 5.1), and then render the view associated with this camera parameter (via volume rendering Eq. 1). The loss computed on the rendered image consists of two parts: image-referenced guidance and reference-free regularization. The referenced loss will enforce \mathbf{V} to have a close appearance with given \mathbf{y} , while the non-referenced term hallucinates the image information with prior knowledge. In the next section, we introduce diffusion model to implement our loss function Eq. 8.

4.2. CLIP-guided Diffusion Priors

Diffusion models [17, 54–56] have achieved undeniable success in image generation. By training on the text-to-image task with a large-scale dataset, diffusion models can precisely represent the distribution over the image manifold conditioned on text description [41, 42, 48]. Therefore, we are motivated to leverage the generative prior of a diffusion model to complement the 3D information. More specifically, we re-parameterize our Eq. 8 with a diffusion model. However, the derived loss function contains both discriminative and generative terms. Inspired by classifier guidance techniques [26, 30, 56], we show that we can leverage the training loss of a diffusion model to surrogate the generative part and utilize CLIP space similarity to model the discriminative part.

Following the derivation in [17] and [32], we lower bound Eq. 8 by:

$$\begin{aligned} & \log p_{\theta}(\mathbf{y}|\mathbf{x}, \mathbf{z}) + \log p_{\theta}(\mathbf{x}|\mathbf{z}) \\ & \geq -\mathbb{E}_{t, \epsilon \sim \mathcal{N}(\mathbf{0}, \mathbf{I})} [\text{KL}(q(\mathbf{x}_{t-1}|\mathbf{x}_t, \mathbf{x}_0) \| p_{\theta}(\mathbf{x}_{t-1}|\mathbf{x}_t, \mathbf{y}, \mathbf{z}))] \\ & = -\mathbb{E}_{t, \epsilon \sim \mathcal{N}(\mathbf{0}, \mathbf{I})} \left[w(t) \|\nabla p_{\theta}(\mathbf{x}_t|\mathbf{y}, \mathbf{z}) - \epsilon\|_2^2 \right], \end{aligned} \quad (9)$$

where $\mathbf{x}_t = \alpha_t \mathbf{x}_0 + \sigma_t \epsilon$ and $w(t)$ is a constant dependent on noise scale α_t and σ_t . The expectation of $t \sim \mathcal{U}\{1, \dots, T\}$ is usually taken over a uniform distribution. We provide detailed derivation in supplementary. At first glance, we may directly plug in the pre-trained denoiser $\epsilon_{\theta}(\mathbf{x}_t; \mathbf{z})$ of a diffusion model to surrogate $\nabla p_{\theta}(\mathbf{x}_t|\mathbf{y}, \mathbf{z})$ similar to [39]. However, note that $p_{\theta}(\mathbf{x}_t|\mathbf{y}, \mathbf{z})$ is also conditioned on the reference image \mathbf{y} , which requires further efforts to inject the reference image information into the diffusion process.

To this end, NeuralLift-360 leverages a Mixed Reference Guidance that guides the diffusion process with a mixture of references. Similar to classifier guidance techniques [26, 30, 32, 56], we rewrite $p_{\theta}(\mathbf{x}_t|\mathbf{y}, \mathbf{z}) = p_{\theta}(\mathbf{y}|\mathbf{x}_t, \mathbf{z})p_{\theta}(\mathbf{x}_t|\mathbf{z})/p_{\theta}(\mathbf{y}_t|\mathbf{z})$, and we adopt classifier-free guidance to model $p_{\theta}(\mathbf{x}_t|\mathbf{z})$, then we can obtain a modified score function [55] as below:

$$\begin{aligned} \tilde{\epsilon}_{\theta}(\mathbf{x}_t; \mathbf{y}, \mathbf{z}) &= (1+w)\epsilon_{\theta}(\mathbf{x}_t; \mathbf{z}) - w\epsilon_{\theta}(\mathbf{x}_t) \\ &+ \sqrt{1-\alpha_t} \nabla \log p_{\theta}(\mathbf{y}|\mathbf{x}_t, \mathbf{z}), \end{aligned} \quad (10)$$

where w is a hyper-parameter that controls the strength of the classifier guidance. We further measure the discrimination with a distance metric on the feature space $p_{\theta}(\mathbf{y}|\mathbf{x}_t, \mathbf{z}) \propto \exp \left[-\phi \left(\frac{\mathbf{x}_t - \sigma_t \tilde{\epsilon}_{\theta}(\mathbf{x}_t; \mathbf{z})}{\alpha_t}, \mathbf{y} \right) \right]$, where $\tilde{\epsilon}_{\theta}(\mathbf{x}_t; \mathbf{z}) = (1+w)\epsilon_{\theta}(\mathbf{x}_t; \mathbf{z}) - w\epsilon_{\theta}(\mathbf{x}_t)$. Specifically, we choose the inner product on the CLIP embedding space [40] as the distance metric, i.e., $\log p_{\theta}(\mathbf{y}|\mathbf{x}_t, \mathbf{z}) \propto -\langle F \left(\frac{\mathbf{x}_t - \sigma_t \tilde{\epsilon}_{\theta}(\mathbf{x}_t)}{\alpha_t} \right), F(\mathbf{y}) \rangle$, which spurs on semantic similarity between denoised rendered image and reference image \mathbf{y} , where F is the CLIP image encoder.

In each training iteration, we alternate two camera pose sampling strategies: (1) we fix a camera pose Φ_0 (i.e., a Delta distribution) as the reference view, and when rendering on that view, we only penalize the RGB differences by modeling $p(\mathbf{y}|h(\mathbf{V}, \Phi), \mathbf{z}) = \mathcal{N}(\mathbf{y}|h(\mathbf{V}, \Phi), \sigma^2 \mathbf{I})$, (2) we stochastically sample camera poses, and adopt the diffusion ELBO (Eq. 9) to estimate the evidence of rendered image together with prior $p_{\theta}(\mathbf{x}|\mathbf{z})$. Combining all together, we can summarize our training loss as below:

$$\begin{aligned} \mathcal{L} &= \frac{1}{\sigma^2} \underbrace{\|h(\mathbf{V}, \Phi_0) - \mathbf{y}\|_2^2}_{\mathcal{L}_{\text{photometric}}} \quad (11) \\ &+ \underbrace{\mathbb{E}_{\Phi, t, \epsilon \sim \mathcal{N}(\mathbf{0}, \mathbf{I})} \left[w(t) \underbrace{\|\tilde{\epsilon}_{\theta}(\alpha_t h(\mathbf{V}, \Phi) + \sigma_t \epsilon | \mathbf{y}, \mathbf{z}) - \epsilon\|_2^2}_{\mathcal{L}_{\text{diff}}} \right]}_{\mathcal{L}_{\text{diff}}}. \end{aligned}$$

Compared with DreamFusion [39], NeuralLift-360’s training objective grounds the 3D scene with the given image which enables the generated scene to have consistent appearance with the specified object.

4.3. Domain Adaption to In-the-wild Images

One main obstacle, however, is assigning a proper text prompt for our reference image. Since the large diffusion

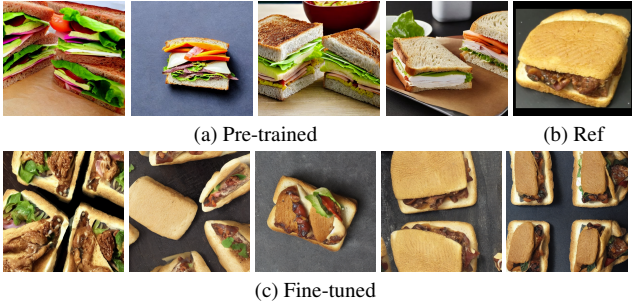


Figure 2. After fine-tuning, our model can generate diverse images similar to the reference image (b) while not identical.

models are mainly trained for the text-to-image task, they usually take a text embedding as conditional input. For images in the wild, it is generally hard to exactly describe an image since images contain more fine-grained information than texts.

Adapting to in-the-wild images requires finetuning the Stable Diffusion model on the reference image. Textual inversion [15] and Dreambooth [49] allow finetuning the Stable Diffusion model on a couple of images to perform subject-driven generation. However, in our case, only one image is available, which severely limits the performance of these methods. Imagic [22] and UniTune [60] support finetuning on a single image, but their goal is to perform real image editing, which can work pretty well even when the diffusion model overfits on the provided image. In our setting, we need the diffusion model to learn to generate images similar to the provided reference but not exactly the same. Otherwise, the NeRF will learn to generate an isotropic surface if the supervision on each view is the same.

We draw inspiration from Pivotal Tuning [47] and Imagic [22] when fine-tuning Stable Diffusion [48] on our own. First, we optimize the CLIP text embedding z so that it suits our reference image y better. During finetuning, we use Eq. 2 to supervise the noise estimate. Since we hope our denoised result should look like the reference image, we also impose a CLIP image loss on the estimated denoised image \hat{x}_0 ,

$$\begin{aligned} \mathcal{L}_{\text{finetune}} = & \mathbb{E}_{t,\epsilon} \left[\|\epsilon - \epsilon_\theta(\mathbf{x}_t; z)\|_2^2 \right] \\ & - \mathbb{E}_{t,\epsilon} \left\langle F \left(\frac{\mathbf{x}_t - \sigma_t \epsilon_\theta(\mathbf{x}_t; z)}{\alpha_t} \right), F(y) \right\rangle, \end{aligned} \quad (12)$$

where $F(\cdot)$ is the pre-trained CLIP image encoder.

Then, we fix the optimized text embedding z^* and fine-tune the model $\epsilon_\theta(\cdot)$ using the same loss function as above. To preserve the generalization ability of the diffusion model, we introduce several augmentations during the finetuning. Specifically, in each iteration, we perform random image-level augmentations such as flip, transpose, shift, scale, and rotate. As shown in Fig. 2, we are able to overcome the overfitting issue and preserve the diffusion

model’s ability to generate diverse similar but not identical contents. Similar to Imagic [22] and UniTune [47], we observe that after finetuning, the optimized text embedding will have an overfitting issue and it is critical to perform interpolation between the original text embedding and the optimized text embedding to preserve the diffusion model’s ability to generate diverse contents. We obtain $z' = \eta z^* + (1 - \eta)z$, where η is a weighting hyperparameter.

During sampling, we aim to amplify the conditional likelihood for our optimized embedding z^* , while decreasing both the unconditional likelihood and the conditional likelihood for the original embedding z . Hence for 50% of all iterations, we use the original Eq. 10, while for the others, we replace the unconditional sampling $\epsilon_\theta(\mathbf{x}_t)$ in Eq. 10 with conditional sampling using the original text embedding z :

$$\begin{aligned} \tilde{\epsilon}_\theta(\mathbf{x}_t; y, z', z) = & (1 + w)\epsilon_\theta(\mathbf{x}_t; z') \\ & - w\epsilon_\theta(\mathbf{x}_t; z) + \sqrt{1 - \alpha_t} \nabla \log p_\theta(y | \mathbf{x}_t, z'), \end{aligned} \quad (13)$$

4.4. Supervision from Rough Depth

Without geometry regularization, it is essentially difficult to obtain a high-quality 3D object with only learning priors. As shown in SinNeRF [70] and DS-NeRF [8], accurate depth information can largely help improve the results’ quality. However, their promising results depend on the 3D consistency of their high-quality depth, and such requirement is not easy to meet in real life.

Despite the exciting progress in monocular depth estimation in the wild, the depth predictions from many recent methods cannot be used to recover the 3D shape. Due to unknown camera baselines and stereoscopic post-processing in data, these methods [7, 25, 44, 64, 69, 72] utilize loss functions invariant to shift and scale or adopt ranking loss that utilizes relative information. Therefore, their results cannot be used to reconstruct plausible 3D scene shapes directly due to unknown depth shifts [74]. Though there are also attempts [74] that improve off-the-shelf depth estimators, they don’t generalize well to unseen objects in the wild.

Since the depth we obtain is imperfect, the absolute depth scale is not reliable enough to recover a high-quality 3D object. Unlike previous depth-supervised NeRFs [8, 70] that can only depend on exact value from the depth map, we make the first attempt to fully utilize the depth information by exploiting the relative ranking information.

Drawing inspiration from [7, 38], we utilize a pairwise depth ranking loss to supervise the rendered depth from our NeRF. In this way, we enforce the depth we rendered to be consistent with the depth from the reference view in terms of internal ranking instead of actual value. The loss is formulated as follows,

$$\mathcal{L}_{\text{ranking}} = \begin{cases} \max(z_{j_k} - z_{i_k}, 0), & r_k \in \{>\} \\ \max(z_{i_k} - z_{j_k}, 0), & r_k \in \{<\} \end{cases} \quad (14)$$

where r_k refers to the pairwise ranking relationship between pixel z_{i_k} and z_{j_k} in the monocular depth estimation. This loss function is used alongside the photo-metric loss and diffusion loss mentioned in Eq. 11 and serves as additional supervision on geometry.

5. Experiments

In this section, we will first describe a unique training recipe that we propose to train our framework, then the implementation details.

5.1. Unique Training Recipe Tailored for NeuralLift-360

Diverse Camera Pose and Intrinsics Sampling During training, we observe that a diverse camera pose and intrinsics are essential for the model to learn a coherent 3D object. If the camera pose is not sampled from a diverse distribution, the 3D object will collapse towards the major viewing directions and thus generate unpleasant results. Specifically, we alter between two pose sampling strategies; (1) we have a fixed camera pose Φ_0 (i.e., a Delta distribution) for the reference view, (2) we uniformly sample the camera rotation on the surface of a unit sphere and then uniformly sample the radius in [0.4, 1.0] to locate the camera. We start with the Delta distribution, and as training progresses, we gradually shift to the other sophisticated camera pose distribution. The camera intrinsics provide additional augmentation on the viewing direction. By uniformly sampling the field of view in [50, 70], we zoom in and out to get different resolution projections for the scene. We also add Gaussian noise to the camera pose sampling phase. Such perturbations help us render more diverse images during training.

Foreground Aware Diffusion Prior ERNIE-ViLG [13] utilizes a weighting mechanism during the training of diffusion models to let the model generate. Using an additional object detection model, their weighted loss forces the model to focus on salient regions. Similarly, we hope to strengthen the guidance on the foreground object region. We propose to weight the score matching distance with the predicted density. Specifically, we penalize the regions with higher density so that our NeRF gains more guidance on the foreground regions. Hence, for each rendered image, we first obtain the bounding box for the non-zero density regions. Then, we extend the $w(t)$ in $\mathcal{L}_{\text{diff}}$ (Eq. 11) into a spatial function:

$$W_{i,j} = \begin{cases} 2, & \text{if } (i, j) \text{ is inside the bounding box} \\ 1, & \text{otherwise.} \end{cases} \quad (15)$$

Geometry Regularization We also include a series of geometry regularizations to avoid undesired artifacts in our 3D object. To avoid foggy and semi-transparent artifacts at the back of the scene, we utilize the orient loss from Ref-NeRF [61] to prevent the surface normals from facing backward from the camera. We also incorporate depth smoothness loss [62], sparsity loss, and distortion loss [3, 58] to avoid the NeRF filling empty space with floaters. Full details for these regularizations are provided in the supplementary material.

Timestep Annealing At the start of training, the quality of the rendered images is poor, and we need the diffusion prior to provide more thorough guidance. As a result, we need to add more noise to perturb the rendered image. As the training progresses, the quality of rendered images gradually improves, and we choose to reduce the timestep range accordingly. By annealing the timestep where we add noise, we are lowering the noise level of the perturbation, and the noise estimate becomes more accurate.

5.2. Evaluation Workflow

We conduct extensive experiments using both text-to-image synthetic images and real-world images. Synthetic images in our experiments are generated using PNDM Sampler [29] with 50 sampling steps. Real images are either from CO3Dv2 dataset [46] or randomly crawled from the Google search engine. For each image, we use a pre-trained background removal framework [1] to segment the foreground objects. Then we obtain their depth using LeRes [73] with the “Boost Your Own depth” [33] strategy. [33] inferences the monocular depth estimation network on multiple patches and then fuses the results for better details. We compare with previous sparse view NeRFs, including Depth-supervised NeRF [8] and SinNeRF [70]. We also compare with DietNeRF [19] that uses CLIP as guidance.

5.3. Comparisons

We present quantitative results in eight scenes. We report the average CLIP distance between rendered image and the reference image as a metric for how well the object is represented. During testing, we use a CLIP model different from training time and evaluate on held out viewing directions with a larger distance-to-origin than training. We render 100 images on each scene for each method. As shown in Tab. 1, our method achieves the best CLIP distance among existing approaches.

We also provide visual comparisons in Fig. 3. Since DS-NeRF and SinNeRF rely on the exact value of the available depth information, their performance using monocular depth estimation is far from satisfactory. It can also be seen that the DietNeRF suffers from unconstrained geometry. Our method, on the other hand, is able to synthesize visually pleasing novel views with 3D consistency.

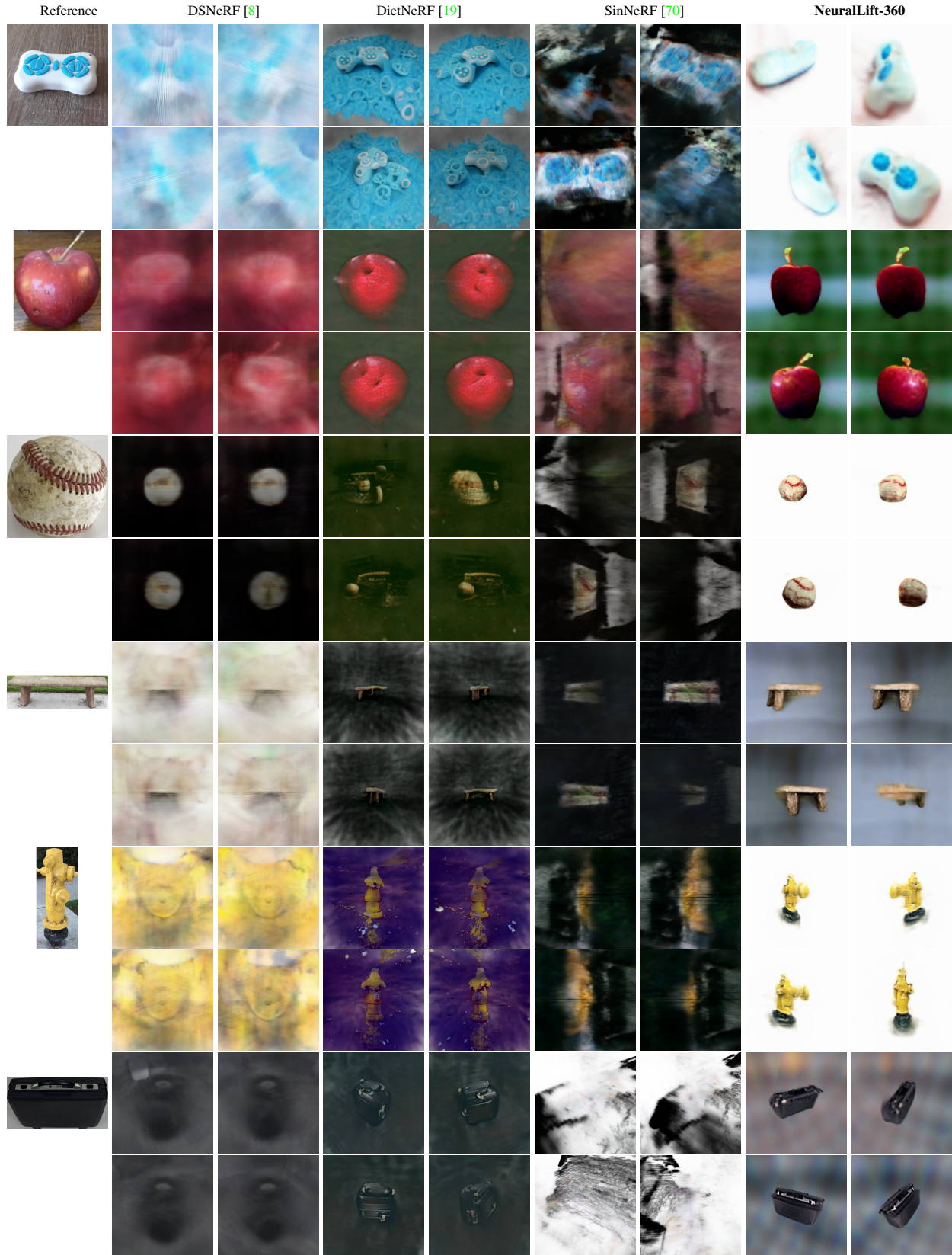


Figure 3. Visual comparisons for novel view synthesis results. We provide **video comparisons** in supplementary.

Table 1. Quantitative evaluation by comparing the proposed method with previous state-of-the-art approaches.

CLIP Distance ↓	Apple	Bench	Baseball	Hydrant	Remote	Suitcase	Statue	Sandwich	Average
DSNeRF [8]	0.5309	0.5447	0.5506	0.6226	0.6441	0.5533	0.5992	0.6110	0.5821
DietNeRF [19]	0.4245	0.5579	0.4545	0.5190	0.5718	0.4890	0.5947	0.5179	0.5162
SinNeRF [70]	0.5192	0.5769	0.6230	0.6343	0.6496	0.5705	0.5605	0.6015	0.5918
NeuralLift-360 (Ours)	0.3914	0.4785	0.3974	0.5146	0.4916	0.4186	0.4411	0.4655	0.4498

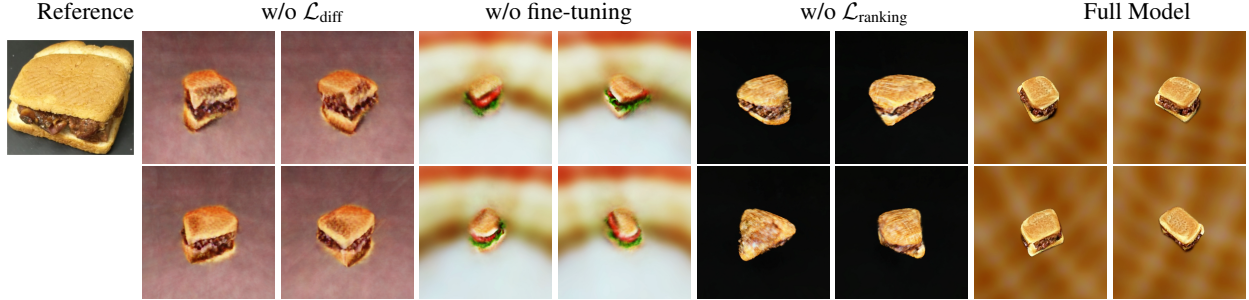


Figure 4. Ablation study on the baseline variants. Given a single reference image, we run different variants to render its 360° views.

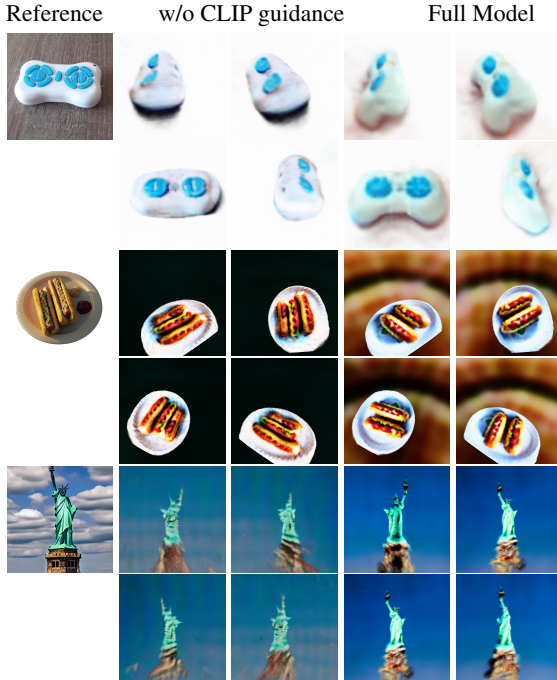


Figure 5. Ablation study on CLIP guidance for the diffusion prior.

5.4. Ablation Study

Variants of supervision. In this section, we perform detailed ablation studies on different components of our framework. “w/o $\mathcal{L}_{\text{ranking}}$ ” replaces the ranking loss with L_1 loss on depth. “w/o $\mathcal{L}_{\text{diff}}$ ” replaces the CLIP guided diffusion prior with CLIP. “w/o fine-tuning” refers to using the pre-trained diffusion model. As shown in Fig. 4, our full model delivers the best performance, while other variants have different issues. “w/o $\mathcal{L}_{\text{ranking}}$ ” relies on the exact value from depth information and suffers from unreliable depth.

“w/o $\mathcal{L}_{\text{diff}}$ ” uses CLIP as a prior, and the optimized result is blurry and collapsed. “w/o fine-tuning” uses a pre-trained diffusion model, since the text prompt is not very accurate, the resulting object has lettuce which doesn’t exist in the reference image.

Effectiveness of CLIP guided diffusion prior We validate the effectiveness of CLIP guidance in our diffusion prior design in Fig. 5. It can be seen that without the CLIP guidance, although the model produces a 3D object, it doesn’t look like the reference image and has a strange shape. In comparison, our full model generates a better shape and looks more similar to the reference image.

6. Conclusions and Future Work

We present NeuralLift-360, a novel framework to lift an in-the-wild 2D photo into a 3D object with 360-degree views. NeuralLift-360 learns probabilistic-driven 3D lifting with CLIP-guided diffusion priors and mitigates the depth errors by a scale-invariant depth ranking loss. Comprehensive experiments are conducted on real and synthetic images, where NeuralLift-360 outperforms the current state-of-the-art methods. While our current implementation is based on Stable Diffusion [48] version 1.4, the framework should also work well with other diffusion models such as Imagen [50] or DALL-E2 [41], once they are open-sourced.

Limitations. Despite the encouraging visual results rendered by NeuralLift-360, the target resolution (128×128) is still behind large generative models [41, 50]. Moreover, challenging cases (e.g., multiple objects with occlusion) are not included in our assumptions, which need to be further explored. Going forward, we will investigate how to expand our method to more general scenarios.

References

- [1] Image background removal. <https://github.com/OHoperHPO/image-background-remove-tool>. 6
- [2] Jonathan T Barron, Ben Mildenhall, Matthew Tancik, Peter Hedman, Ricardo Martin-Brualla, and Pratul P Srinivasan. Mip-nerf: A multiscale representation for anti-aliasing neural radiance fields. In *Proceedings of the IEEE/CVF International Conference on Computer Vision*, pages 5855–5864, 2021. 2
- [3] Jonathan T Barron, Ben Mildenhall, Dor Verbin, Pratul P Srinivasan, and Peter Hedman. Mip-nerf 360: Unbounded anti-aliased neural radiance fields. In *Proceedings of the IEEE/CVF Conference on Computer Vision and Pattern Recognition*, pages 5470–5479, 2022. 2, 6
- [4] Angel X. Chang, Thomas Funkhouser, Leonidas Guibas, Pat Hanrahan, Qixing Huang, Zimo Li, Silvio Savarese, Manolis Savva, Shuran Song, Hao Su, Jianxiong Xiao, Li Yi, and Fisher Yu. ShapeNet: An Information-Rich 3D Model Repository. Technical Report arXiv:1512.03012 [cs.GR], Stanford University — Princeton University — Toyota Technological Institute at Chicago, 2015. 1
- [5] Anpei Chen, Zexiang Xu, Fuqiang Zhao, Xiaoshuai Zhang, Fanbo Xiang, Jingyi Yu, and Hao Su. Mvsnerf: Fast generalizable radiance field reconstruction from multi-view stereo. In *Proceedings of the IEEE/CVF International Conference on Computer Vision*, pages 14124–14133, 2021. 2
- [6] Tianlong Chen, Peihao Wang, Zhiwen Fan, and Zhangyang Wang. Aug-nerf: Training stronger neural radiance fields with triple-level physically-grounded augmentations. In *Proceedings of the IEEE/CVF Conference on Computer Vision and Pattern Recognition*, pages 15191–15202, 2022. 2
- [7] Weifeng Chen, Zhao Fu, Dawei Yang, and Jia Deng. Single-image depth perception in the wild. *Advances in neural information processing systems*, 29, 2016. 5
- [8] Kangle Deng, Andrew Liu, Jun-Yan Zhu, and Deva Ramanan. Depth-supervised nerf: Fewer views and faster training for free. In *Proceedings of the IEEE/CVF Conference on Computer Vision and Pattern Recognition*, pages 12882–12891, 2022. 1, 5, 6, 7, 8
- [9] Jean-Denis Durou, Maurizio Falcone, and Manuela Sagona. Numerical methods for shape-from-shading: A new survey with benchmarks. *Computer Vision and Image Understanding*, 109(1):22–43, 2008. 1
- [10] Haoqiang Fan, Hao Su, and Leonidas J Guibas. A point set generation network for 3d object reconstruction from a single image. In *Proceedings of the IEEE conference on computer vision and pattern recognition*, pages 605–613, 2017. 1
- [11] Zhiwen Fan, Yifan Jiang, Peihao Wang, Xinyu Gong, Dejia Xu, and Zhangyang Wang. Unified implicit neural stylization. *arXiv preprint arXiv:2204.01943*, 2022. 2
- [12] Paolo Favaro and Stefano Soatto. A geometric approach to shape from defocus. *IEEE Transactions on Pattern Analysis and Machine Intelligence*, 27(3):406–417, 2005. 1
- [13] Zhida Feng, Zhenyu Zhang, Xintong Yu, Yewei Fang, Lanxin Li, Xuyi Chen, Yuxiang Lu, Jiaxiang Liu, Weichong Yin, Shikun Feng, et al. Ernie-vilg 2.0: Improving text-to-image diffusion model with knowledge-enhanced mixture-of-denoising-experts. *arXiv preprint arXiv:2210.15257*, 2022. 6
- [14] Sara Fridovich-Keil, Alex Yu, Matthew Tancik, Qinrong Chen, Benjamin Recht, and Angjoo Kanazawa. Plenoxels: Radiance fields without neural networks. In *Proceedings of the IEEE/CVF Conference on Computer Vision and Pattern Recognition*, pages 5501–5510, 2022. 2
- [15] Rinon Gal, Yuval Alaluf, Yuval Atzmon, Or Patashnik, Amit H Bermano, Gal Chechik, and Daniel Cohen-Or. An image is worth one word: Personalizing text-to-image generation using textual inversion. *arXiv preprint arXiv:2208.01618*, 2022. 5
- [16] Yuan-Chen Guo, Di Kang, Linchao Bao, Yu He, and Song-Hai Zhang. Nerfren: Neural radiance fields with reflections. In *Proceedings of the IEEE/CVF Conference on Computer Vision and Pattern Recognition*, pages 18409–18418, 2022. 2
- [17] Jonathan Ho, Ajay Jain, and Pieter Abbeel. Denoising diffusion probabilistic models. *Advances in Neural Information Processing Systems*, 33:6840–6851, 2020. 3, 4
- [18] Ajay Jain, Ben Mildenhall, Jonathan T Barron, Pieter Abbeel, and Ben Poole. Zero-shot text-guided object generation with dream fields. In *Proceedings of the IEEE/CVF Conference on Computer Vision and Pattern Recognition*, pages 867–876, 2022. 2
- [19] Ajay Jain, Matthew Tancik, and Pieter Abbeel. Putting nerf on a diet: Semantically consistent few-shot view synthesis. In *Proceedings of the IEEE/CVF International Conference on Computer Vision*, pages 5885–5894, 2021. 1, 6, 7, 8
- [20] Varun Jampani, Huiwen Chang, Kyle Sargent, Abhishek Kar, Richard Tucker, Michael Krainin, Dominik Kaeser, William T Freeman, David Salesin, Brian Curless, et al. Slide: Single image 3d photography with soft layering and depth-aware inpainting. In *Proceedings of the IEEE/CVF International Conference on Computer Vision*, pages 12518–12527, 2021. 2
- [21] Adrian Johnston, Ravi Garg, Gustavo Carneiro, Ian Reid, and Anton van den Hengel. Scaling cnns for high resolution volumetric reconstruction from a single image. In *Proceedings of the IEEE International Conference on Computer Vision Workshops*, pages 939–948, 2017. 1
- [22] Bahjat Kawar, Shiran Zada, Oran Lang, Omer Tov, Huiwen Chang, Tali Dekel, Inbar Mosseri, and Michal Irani. Imagic: Text-based real image editing with diffusion models. *arXiv preprint arXiv:2210.09276*, 2022. 5
- [23] Diederik Kingma, Tim Salimans, Ben Poole, and Jonathan Ho. Variational diffusion models. *Advances in neural information processing systems*, 34:21696–21707, 2021. 3
- [24] Hyung-Kwon Ko, Gwanmo Park, Hyeon Jeon, Jaemin Jo, Juho Kim, and Jinwook Seo. Large-scale text-to-image generation models for visual artists’ creative works. *arXiv preprint arXiv:2210.08477*, 2022. 2
- [25] Manuel Lang, Alexander Hornung, Oliver Wang, Steven Poulakos, Aljoscha Smolic, and Markus Gross. Nonlinear disparity mapping for stereoscopic 3d. *ACM Transactions on Graphics (TOG)*, 29(4):1–10, 2010. 5

- [26] Yann LeCun, Sumit Chopra, Raia Hadsell, M Ranzato, and Fujie Huang. A tutorial on energy-based learning. *Predicting structured data*, 1(0), 2006. 4
- [27] Zhengqi Li and Noah Snavely. Megadepth: Learning single-view depth prediction from internet photos. In *Proceedings of the IEEE Conference on Computer Vision and Pattern Recognition*, pages 2041–2050, 2018. 1
- [28] Kai-En Lin, Lin Yen-Chen, Wei-Sheng Lai, Tsung-Yi Lin, Yi-Chang Shih, and Ravi Ramamoorthi. Vision transformer for nerf-based view synthesis from a single input image. *arXiv preprint arXiv:2207.05736*, 2022. 2
- [29] Luping Liu, Yi Ren, Zhijie Lin, and Zhou Zhao. Pseudo numerical methods for diffusion models on manifolds. *arXiv preprint arXiv:2202.09778*, 2022. 6
- [30] Xihui Liu, Dong Huk Park, Samaneh Azadi, Gong Zhang, Arman Chopikyan, Yuxiao Hu, Humphrey Shi, Anna Rohrbach, and Trevor Darrell. More control for free! image synthesis with semantic diffusion guidance. 2021. 4
- [31] Yuan Liu, Sida Peng, Lingjie Liu, Qianqian Wang, Peng Wang, Christian Theobalt, Xiaowei Zhou, and Wenping Wang. Neural rays for occlusion-aware image-based rendering. In *Proceedings of the IEEE/CVF Conference on Computer Vision and Pattern Recognition*, pages 7824–7833, 2022. 2
- [32] Calvin Luo. Understanding diffusion models: A unified perspective. *arXiv preprint arXiv:2208.11970*, 2022. 4
- [33] S. Mahdi H. Miangoleh, Sebastian Dille, Long Mai, Sylvain Paris, and Yağız Aksoy. Boosting monocular depth estimation models to high-resolution via content-adaptive multi-resolution merging. 2021. 6
- [34] Ben Mildenhall, Pratul P Srinivasan, Matthew Tancik, Jonathan T Barron, Ravi Ramamoorthi, and Ren Ng. Nerf: Representing scenes as neural radiance fields for view synthesis. In *European conference on computer vision*, pages 405–421. Springer, 2020. 2, 3
- [35] Ben Mildenhall, Pratul P Srinivasan, Matthew Tancik, Jonathan T Barron, Ravi Ramamoorthi, and Ren Ng. Nerf: Representing scenes as neural radiance fields for view synthesis. *Communications of the ACM*, 65(1):99–106, 2021. 1
- [36] Fangzhou Mu, Jian Wang, Yicheng Wu, and Yin Li. 3d photo stylization: Learning to generate stylized novel views from a single image. In *Proceedings of the IEEE/CVF Conference on Computer Vision and Pattern Recognition*, pages 16273–16282, 2022. 2
- [37] Thomas Müller, Alex Evans, Christoph Schied, and Alexander Keller. Instant neural graphics primitives with a multiresolution hash encoding. *arXiv preprint arXiv:2201.05989*, 2022. 2, 3
- [38] Georgios Pavlakos, Xiaowei Zhou, and Kostas Daniilidis. Ordinal depth supervision for 3d human pose estimation. In *Proceedings of the IEEE Conference on Computer Vision and Pattern Recognition*, pages 7307–7316, 2018. 5
- [39] Ben Poole, Ajay Jain, Jonathan T Barron, and Ben Mildenhall. Dreamfusion: Text-to-3d using 2d diffusion. *arXiv preprint arXiv:2209.14988*, 2022. 2, 4
- [40] Alec Radford, Jong Wook Kim, Chris Hallacy, Aditya Ramesh, Gabriel Goh, Sandhini Agarwal, Girish Sastry, Amanda Askell, Pamela Mishkin, Jack Clark, et al. Learning transferable visual models from natural language supervision. In *International Conference on Machine Learning*, pages 8748–8763. PMLR, 2021. 2, 4
- [41] Aditya Ramesh, Prafulla Dhariwal, Alex Nichol, Casey Chu, and Mark Chen. Hierarchical text-conditional image generation with clip latents. *arXiv preprint arXiv:2204.06125*, 2022. 2, 4, 8
- [42] Aditya Ramesh, Mikhail Pavlov, Gabriel Goh, Scott Gray, Chelsea Voss, Alec Radford, Mark Chen, and Ilya Sutskever. Zero-shot text-to-image generation. In *International Conference on Machine Learning*, pages 8821–8831. PMLR, 2021. 4
- [43] René Ranftl, Alexey Bochkovskiy, and Vladlen Koltun. Vision transformers for dense prediction. In *Proceedings of the IEEE/CVF International Conference on Computer Vision*, pages 12179–12188, 2021. 1
- [44] René Ranftl, Katrin Lasinger, David Hafner, Konrad Schindler, and Vladlen Koltun. Towards robust monocular depth estimation: Mixing datasets for zero-shot cross-dataset transfer. *IEEE transactions on pattern analysis and machine intelligence*, 2020. 1, 2, 5
- [45] Christian Reiser, Songyou Peng, Yiyi Liao, and Andreas Geiger. Kilonerf: Speeding up neural radiance fields with thousands of tiny mlps. In *Proceedings of the IEEE/CVF International Conference on Computer Vision*, pages 14335–14345, 2021. 2
- [46] Jeremy Reizenstein, Roman Shapovalov, Philipp Henzler, Luca Sbordone, Patrick Labatut, and David Novotny. Common objects in 3d: Large-scale learning and evaluation of real-life 3d category reconstruction. In *International Conference on Computer Vision*, 2021. 6
- [47] Daniel Roich, Ron Mokady, Amit H Bermano, and Daniel Cohen-Or. Pivotal tuning for latent-based editing of real images. *ACM Transactions on Graphics (TOG)*, 42(1):1–13, 2022. 5
- [48] Robin Rombach, Andreas Blattmann, Dominik Lorenz, Patrick Esser, and Björn Ommer. High-resolution image synthesis with latent diffusion models. In *Proceedings of the IEEE/CVF Conference on Computer Vision and Pattern Recognition*, pages 10684–10695, 2022. 2, 4, 5, 8
- [49] Nataniel Ruiz, Yuanzhen Li, Varun Jampani, Yael Pritch, Michael Rubinstein, and Kfir Aberman. Dreambooth: Fine tuning text-to-image diffusion models for subject-driven generation. *arXiv preprint arXiv:2208.12242*, 2022. 5
- [50] Chitwan Saharia, William Chan, Saurabh Saxena, Lala Li, Jay Whang, Emily Denton, Seyed Kamvar Seyed Ghasemipour, Burcu Karagol Ayan, S Sara Mahdavi, Rapha Gontijo Lopes, et al. Photorealistic text-to-image diffusion models with deep language understanding. *arXiv preprint arXiv:2205.11487*, 2022. 2, 8
- [51] Shunsuke Saito, Zeng Huang, Ryota Natsume, Shigeo Morigi, Angjoo Kanazawa, and Hao Li. Pifu: Pixel-aligned implicit function for high-resolution clothed human digitization. In *Proceedings of the IEEE/CVF International Conference on Computer Vision*, pages 2304–2314, 2019. 1
- [52] Meng-Li Shih, Shih-Yang Su, Johannes Kopf, and Jia-Bin Huang. 3d photography using context-aware layered depth

- inpainting. In *Proceedings of the IEEE/CVF Conference on Computer Vision and Pattern Recognition*, pages 8028–8038, 2020. 1, 2
- [53] Jascha Sohl-Dickstein, Eric Weiss, Niru Maheswaranathan, and Surya Ganguli. Deep unsupervised learning using nonequilibrium thermodynamics. In *International Conference on Machine Learning*, pages 2256–2265. PMLR, 2015. 3
- [54] Jiaming Song, Chenlin Meng, and Stefano Ermon. Denoising diffusion implicit models. *arXiv preprint arXiv:2010.02502*, 2020. 3, 4
- [55] Yang Song and Stefano Ermon. Generative modeling by estimating gradients of the data distribution. *Advances in Neural Information Processing Systems*, 32, 2019. 4
- [56] Yang Song, Jascha Sohl-Dickstein, Diederik P Kingma, Abhishek Kumar, Stefano Ermon, and Ben Poole. Score-based generative modeling through stochastic differential equations. *arXiv preprint arXiv:2011.13456*, 2020. 3, 4
- [57] Mohammed Suhail, Carlos Esteves, Leonid Sigal, and Ameesh Makadia. Light field neural rendering. In *Proceedings of the IEEE/CVF Conference on Computer Vision and Pattern Recognition*, pages 8269–8279, 2022. 2
- [58] Cheng Sun, Min Sun, and Hwann-Tzong Chen. Improved direct voxel grid optimization for radiance fields reconstruction. *arxiv cs.GR 2206.05085*, 2022. 6
- [59] Cheng Sun, Min Sun, and Hwann-Tzong Chen. Direct voxel grid optimization: Super-fast convergence for radiance fields reconstruction. In *Proceedings of the IEEE/CVF Conference on Computer Vision and Pattern Recognition*, pages 5459–5469, 2022. 2
- [60] Dani Valevski, Matan Kalman, Yossi Matias, and Yaniv Leviathan. Unitune: Text-driven image editing by fine tuning an image generation model on a single image. *arXiv preprint arXiv:2210.09477*, 2022. 5
- [61] Dor Verbin, Peter Hedman, Ben Mildenhall, Todd Zickler, Jonathan T Barron, and Pratul P Srinivasan. Ref-nerf: Structured view-dependent appearance for neural radiance fields. In *2022 IEEE/CVF Conference on Computer Vision and Pattern Recognition (CVPR)*, pages 5481–5490. IEEE, 2022. 2, 6
- [62] Chaoyang Wang, José Miguel Buenaposada, Rui Zhu, and Simon Lucey. Learning depth from monocular videos using direct methods. In *Proceedings of the IEEE conference on computer vision and pattern recognition*, pages 2022–2030, 2018. 6
- [63] Can Wang, Menglei Chai, Mingming He, Dongdong Chen, and Jing Liao. Clip-nerf: Text-and-image driven manipulation of neural radiance fields. In *Proceedings of the IEEE/CVF Conference on Computer Vision and Pattern Recognition*, pages 3835–3844, 2022. 2
- [64] Chaoyang Wang, Simon Lucey, Federico Perazzi, and Oliver Wang. Web stereo video supervision for depth prediction from dynamic scenes. In *2019 International Conference on 3D Vision (3DV)*, pages 348–357. IEEE, 2019. 5
- [65] Lizhen Wang, Xiaochen Zhao, Tao Yu, Songtao Wang, and Yebin Liu. Normalgan: Learning detailed 3d human from a single rgbd image. In *European Conference on Computer Vision*, pages 430–446. Springer, 2020. 1
- [66] Nanyang Wang, Yinda Zhang, Zhuwen Li, Yanwei Fu, Wei Liu, and Yu-Gang Jiang. Pixel2mesh: Generating 3d mesh models from single rgb images. In *Proceedings of the European conference on computer vision (ECCV)*, pages 52–67, 2018. 1
- [67] Qianqian Wang, Zhicheng Wang, Kyle Genova, Pratul P Srinivasan, Howard Zhou, Jonathan T Barron, Ricardo Martin-Brualla, Noah Snavely, and Thomas Funkhouser. Ibrnet: Learning multi-view image-based rendering. In *Proceedings of the IEEE/CVF Conference on Computer Vision and Pattern Recognition*, pages 4690–4699, 2021. 2
- [68] Jiajun Wu, Yifan Wang, Tianfan Xue, Xingyuan Sun, Bill Freeman, and Josh Tenenbaum. Marrnet: 3d shape reconstruction via 2.5 d sketches. *Advances in neural information processing systems*, 30, 2017. 1
- [69] Ke Xian, Chunhua Shen, Zhiguo Cao, Hao Lu, Yang Xiao, Ruibo Li, and Zhenbo Luo. Monocular relative depth perception with web stereo data supervision. In *Proceedings of the IEEE Conference on Computer Vision and Pattern Recognition*, pages 311–320, 2018. 5
- [70] Dejia Xu, Yifan Jiang, Peihao Wang, Zhiwen Fan, Humphrey Shi, and Zhangyang Wang. Sinnerf: Training neural radiance fields on complex scenes from a single image. *arXiv preprint arXiv:2204.00928*, 2022. 1, 2, 5, 6, 7, 8
- [71] Yao Yao, Zixin Luo, Shiwei Li, Tian Fang, and Long Quan. Mvsnet: Depth inference for unstructured multi-view stereo. In *Proceedings of the European conference on computer vision (ECCV)*, pages 767–783, 2018. 1
- [72] Wei Yin, Xinlong Wang, Chunhua Shen, Yifan Liu, Zhi Tian, Songcen Xu, Changming Sun, and Dou Renyin. Diversedepth: Affine-invariant depth prediction using diverse data. *arXiv preprint arXiv:2002.00569*, 2020. 5
- [73] Wei Yin, Jianming Zhang, Oliver Wang, Simon Niklaus, Long Mai, Simon Chen, and Chunhua Shen. Learning to recover 3d scene shape from a single image. In *Proc. IEEE Conf. Comp. Vis. Patt. Recogn. (CVPR)*, 2021. 1, 6
- [74] Wei Yin, Jianming Zhang, Oliver Wang, Simon Niklaus, Long Mai, Simon Chen, and Chunhua Shen. Learning to recover 3d scene shape from a single image. In *Proceedings of the IEEE/CVF Conference on Computer Vision and Pattern Recognition*, pages 204–213, 2021. 5
- [75] Alex Yu, Vickie Ye, Matthew Tancik, and Angjoo Kanazawa. pixelnerf: Neural radiance fields from one or few images. In *Proceedings of the IEEE/CVF Conference on Computer Vision and Pattern Recognition*, pages 4578–4587, 2021. 1, 2
- [76] Jiahui Yu, Zhe Lin, Jimei Yang, Xiaohui Shen, Xin Lu, and Thomas S Huang. Free-form image inpainting with gated convolution. In *Proceedings of the IEEE/CVF international conference on computer vision*, pages 4471–4480, 2019. 2